Magnetic field pitch angle and perpendicular velocity measurements from multi-point time-delay estimation of poloidal correlation reflectometry

D. Prisiazhniuk[1,2], A. Krämer-Flecken[3], G.D. Conway[1], T. Happel[1], A. Lebschy[1,2], P. Manz[1,2], V. Nikolaeva[1,2,4], U. Stroth[1,2] and the ASDEX Upgrade Team[1]

[1]Max-Planck-Institut für Plasmaphysik, Boltzmannstraße 2, 85748 Garching, Germany

[2]Physik-Department E28, Technische Universität München, 85748 Garching, Germany

[3]Institut für Energieforschung - Plasmaphysik, Forschungszentrum Jülich, Germany

[4]Instituto de Plasmas e Fusão Nuclear, Instituto Superior Técnico, Av. Rovisco Pais 1, 1049-001 Lisboa, Portugal

Abstract. In fusion machines turbulent eddies are expected to be aligned with the direction of the magnetic field lines and to propagate in the perpendicular direction. Time delay measurements of density fluctuations can be used for the calculation of magnetic field pitch angle α and perpendicular velocity $v_\perp$ profiles. The method is applied to poloidal correlation reflectometry installed at ASDEX Upgrade and TEXTOR, which measure density fluctuations from poloidally and toroidally separated antennas. Validation of the method is achieved by comparison of the perpendicular velocity (composed of the ExB drift and the phase velocity of turbulence $v_\perp = v_{E\times B} + v_{ph}$), with Doppler reflectometry measurements, and with neoclassic fluid calculations. An important condition for the application of the method is the presence of turbulence with sufficiently long decorrelation time. It is shown that at the shear layer the decorrelation time is reduced, limiting the application of the method. The magnetic field pitch angle measured by this method shows the expected dependence on the magnetic field, plasma current and radial position. The profile of the pitch angle reproduces the expected shape and values. However, a comparison with the equilibrium reconstruction code CLISTE suggests an additional inclination of turbulent eddies at the pedestal position (2–3°). This additional angle decreases towards core and at the edge.

PACS numbers: 52.35.Ra, 52.55.-s, 52.70.-m, 52.70.Gw, 52.30.Fi, 52.30.-q, 52.55.Fa

Submitted to: *PPCF*

E-mail: dmitrii.prisiazhniuk@ipp.mpg.de

1. Introduction

In current driven high temperature fusion plasmas, such as tokamaks, the radial profile of the plasma current and the corresponding magnetic field structure are important parameters. They influence the plasma confinement stability and transport. Knowledge of the current profile is particularly important for studying bootstrap current dependences, internal barrier formation, and the physics of magnetohydrodynamics (MHD) modes [1, 2, 3]. The peeling-balloning stability of the plasma pedestal in high confinement discharges and the dynamics of the Edge-Localized-Mode (ELM) cycle are also affected by the current profile dynamics [4]. In a tokamak the combination of the externally applied toroidal magnetic field B_t and the poloidal magnetic field B_p generated by the plasma current I_p creates a helical field line structure. The slope of the magnetic field lines depends therefore on the poloidal magnetic field and the related plasma current I_p. This slope is called the magnetic field pitch angle defined as $\alpha = \arctan(B_p/B_t)$.

Typically, Motional Stark Emission (MSE) diagnostics are used to estimate the α profile [5] in present devices. However, this diagnostic technique requires optical elements within the vacuum vessel, which can suffer erosion and deposition - thus limiting the accuracy and lifetime of the diagnostic. An alternative approach, based on the measurement of the Faraday rotation of a laser beam passing through the plasma [6], however, lacks radial resolution and a pitch angle profile can only be obtained from multiple laser chords and subsequent Abel inversion. Future fusion devices will require a more robust approach to deduce the pitch angle profile.

Here we report on the determination of the magnetic field pitch angle and turbulence perpendicular velocity from multi-point time delay estimation of turbulent eddies measured by Poloidal Correlation Reflectometry. The advantages of this method are a reduced effort and space for the antenna installation and insensitivity to material erosion and radiation. This application has potential for future fusion devices such as ITER and DEMO. The method itself is based on the measurement of the propagation of density fluctuation from poloidally and toroidally separated antennas combinations that allow the extraction of the inclination of turbulent structures and their propagation velocity. To zeroth order, the turbulent structures are expected to be aligned in the direction of the magnetic field thus allowing estimation of the pitch angle profile. In this paper the method is applied to the ASDEX Upgrade and TEXTOR tokamaks and its accuracy and limitations are discussed.

The paper is organized as follows: in section 2 the method of extracting the pitch angle and perpendicular velocity from multi-point time delay measurements is introduced and the necessary assumptions and the accuracy of the method are discussed. In section 3 the Poloidal Correlation Reflectometry (PCR) diagnostic is described in general, and specifically the multi-antenna cluster diagnostic installed at ASDEX Upgrade (AUG) and TEXTOR tokamaks. The estimation of the position of reflection obtained from beam tracing code TORBEAM, as well as the sensitivity of the spatial separation between

points for different magnetic configuration are discussed. In section 4 the diagnostic is applied to pitch angle and perpendicular velocity studies at TEXTOR and AUG. The last section summarizes results and presents an outlook for future experiments and applications of the method.

2. Magnetic field pitch angle and perpendicular velocity extraction from multi-point time-delay estimations

2.1. Time delay estimation in tokamaks

Time delay estimation is a widely used tool for obtaining flow velocity measurements from the spatiotemporal correlation of density or temperature fluctuations [7, 8]. The maximum of the cross-correlation function (CCF) between two spatially separated measurements yields a time delay τ_m, which under certain conditions is proportional to the fluctuation propagation velocity $\vec{v}$. In fusion plasmas the correlation of small-scale turbulence is generally used to determine a time delay from poloidally and toroidally separated measurements. The CCF of the density fluctuating component about their mean values in turbulent fields is defined as [9]

$$\rho(\vec{\varepsilon},\tau) = \frac{\langle \delta n(\vec{r},t)\delta n(\vec{r}+\vec{\varepsilon},t+\tau)\rangle}{\sqrt{\langle \delta n^2(\vec{r},t)\rangle}\sqrt{\langle \delta n^2(\vec{r}+\vec{\varepsilon},t+\tau)\rangle}}\,, \tag{1}$$

where $\vec{\varepsilon}$ is a spatial separation vector and τ is a time separation. The CCF for other fluctuating turbulence properties, such as temperature, are expressed similarly.

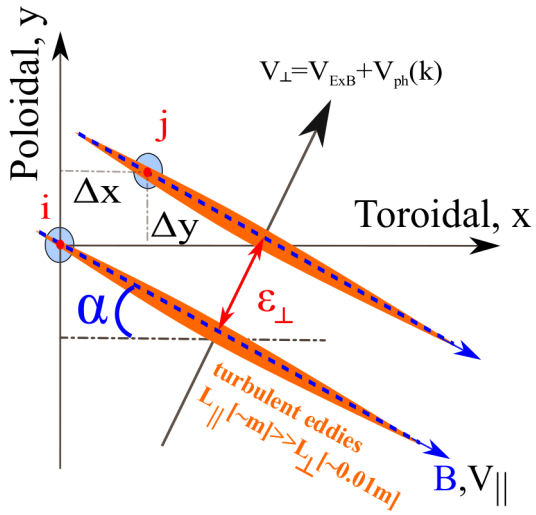

Figure 1. Schematic representation of 2 point time delay measurements. Turbulent eddies (orange) aligned parallel to the magnetic field move in the perpendicular direction resulting in the time delay between detecting volumes i and j.

To first order, turbulent structures are expected to be strongly elongated with the

direction of the helical magnetic field i.e. inclined to the toroidal direction. On a magnetic surface, turbulent eddies have two velocity components. One parallel to the magnetic field $v_{||}$ and one perpendicular to the magnetic field composed of the $E\times B$ drift and the phase velocity of the turbulent structures $v_\perp = (E\times B)/B^2 + v_{ph}(k_\perp)$ (c.f. figure 1), where $k_\perp$ is the perpendicular wavenumber. While propagating, the turbulence eddies additionally mutate with an effective decorrelation time τ_d. Using the elliptical approximation at small separations [10, 11, 12, 13] for the turbulence having a Gaussian distribution, both in space and time, the point cross correlation on the magnetic surface can be expressed as

$$\rho(\varepsilon_\parallel, \varepsilon_\perp, \tau) = \exp\left(-\frac{(\varepsilon_\parallel - v_\parallel\tau)^2}{l_{||}^2} - \frac{(\varepsilon_\perp - v_\perp\tau)^2}{l_\perp^2} - \frac{\tau^2}{\tau_d^2}\right). \tag{2}$$

Here $l_\parallel$ and $l_\perp$ denote the parallel and perpendicular fluctuation correlation lengths, $\varepsilon_\parallel$ and $\varepsilon_\perp$ the parallel and perpendicular separations between the measured volumes and τ the separation in time. Such a CCF is evidently valid for small separations $\vec{\varepsilon}$ and τ and satisfy $\rho'_{\varepsilon_i}(0,0) = 0$ due to homogeneity of the space and $\rho'_\tau(0,0) = 0$ due to stationary [12]. The CCF is also applicable to experimental results presented in section 4. In principle both velocities, $v_\parallel$ and $v_\perp$, should be taken into account during the extraction of velocities from time delay measurements. However, for comparable separations in parallel and perpendicular directions $\varepsilon_\perp \approx \varepsilon_\parallel$ the parallel velocity can be neglected in time delay measurements when the following is met

$$\gamma = \frac{v_{||}}{v_\perp}\frac{l_\perp}{l_{||}} \ll 1. \tag{3}$$

Condition (3) is fulfilled in toroidally confined plasmas due to the fact that the parallel correlation length of measured structures $l_{||}$ (several meters) [14, 15, 16, 17] is significantly longer than the perpendicular correlation length $l_\perp$ (some centimeters). This means that the parallel velocity can only affect the time delay measurements if $v_{||} \gtrsim 10^2 v_\perp$. This is rarely the case for typical L-mode plasmas, however, possible where $v_\perp \approx 0$ (e.g. in the edge shear region, where $v_\perp$ changes sign). In the following analyses we neglect the parallel propagation. In this case the CCF simplifies to

$$\rho(\varepsilon_\perp, \tau) = \exp\left(-\frac{(\varepsilon_\perp - v_\perp\tau)^2}{l_\perp^2} - \frac{\tau^2}{\tau_d^2}\right). \tag{4}$$

In the case of arbitrary measuring positions on the magnetic surface the separation perpendicular to the magnetic field B can be calculated as

$$\varepsilon_\perp(\Delta x, \Delta y, \alpha) = (\Delta y + \Delta x \tan(\alpha))\cos(\alpha), \tag{5}$$

here Δx and Δy denote the separation between detecting volumes in the toroidal and poloidal directions respectively and α denotes the value of the magnetic field pitch angle (figure 1). In figure 2 an example of $\rho(\varepsilon_\perp, \tau)$ for different perpendicular separations is shown using typical values of $\tau_d = 7$ μs, $l_\perp = 1.5$ cm and $v_\perp = 3$ km/s. The maximum of CCF $\rho_m = \max_\tau(|\rho(\varepsilon_\perp, \tau)|)$ (red points) decreases with separation, due to the decorrelation of the turbulent structures while propagating. The decorrelation

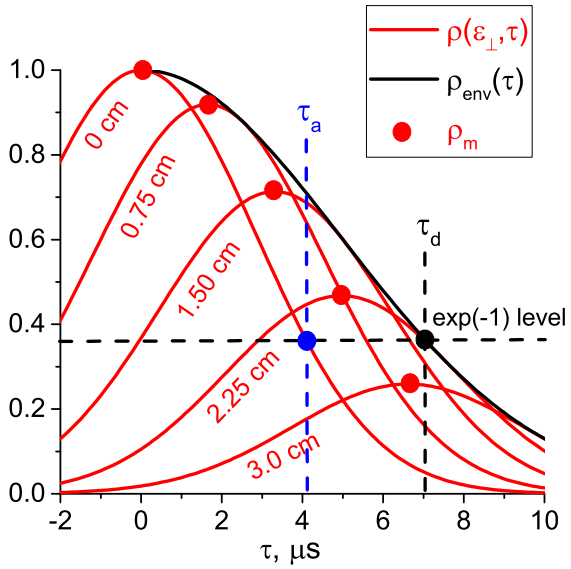

Figure 2. Cross-correlation function of density fluctuations for different perpendicular separations.

curve is described by the envelope function $\rho_{env}(\tau) = \exp(-\tau^2/\tau_d^2)$ (black curve) with the decorrelation time τ_d. The maximum correlation time delays

$$\tau_m(\varepsilon_\perp) = \arg\max_\tau(|\rho(\varepsilon_\perp, \tau)|) = \frac{\varepsilon_\perp}{v_\perp}\left(1 + \frac{l_\perp^2}{v_\perp^2\tau_d^2}\right)^{-1} \tag{6}$$

(red points) are increasing with separation. It is important to note that the measurement of time delays τ_m are difficult when they exceed the decorrelation time τ_d of the turbulence due to low levels of correlation. This is limits the maximal separation between the measured volumes.

For the case of infinite decorrelation time $\tau_d = \infty$, a ratio of the time delay and the separation $\tau_m(\varepsilon_\perp)/\varepsilon_\perp$ depends only on the perpendicular velocity. However, for the case of a finite decorrelation time, this ratio is not only a function of $v_\perp$, but also depends on $l_\perp$ and τ_d. The perpendicular velocity can be estimated if the autocorrelation time $\rho(0, \tau_a) = \rho(0, 0)/e$ and the decorrelation time $\rho_{env}(\tau_d) = \rho_{env}(0)/e$ are known. Using equation (4) the autocorrelation time can be expressed as

$$\tau_a = \frac{(l_\perp/v_\perp)\tau_d}{\sqrt{l_\perp^2/v_\perp^2 + \tau_d^2}}. \tag{7}$$

Combining equations (6) and (7) we can show that the time delay can be expressed via τ_a and τ_d as

$$\tau_m(\varepsilon_\perp) = \frac{\varepsilon_\perp}{v_\perp}\left(1 - \frac{\tau_a^2}{\tau_d^2}\right). \tag{8}$$

This relationship allows us to calculate the perpendicular velocity as

$$v_\perp = \frac{\varepsilon_\perp}{\tau_m(\varepsilon_\perp)}\left(1 - \frac{\tau_a^2}{\tau_d^2}\right). \tag{9}$$

Although, the autocorrelation time depends on $l_\perp$, τ_d and $v_\perp$, both τ_a and τ_d can be measured experimentally, as shown in figure 2 (blue and black point). This measurement methodology is similar to one obtained by Briggs [10] and applied to plasmas in [11]. Summarizing, the measurement of $v_\perp$ from time delay analyses using this method can be achieved when the following conditions are fulfilled:

(i) If structures are aligned in the direction of the magnetic field and the value of magnetic field pitch angle α is known.

(ii) If the value of the time delay τ_m between two measured volumes does not exceed the decorrelation time τ_d of the turbulence i.e. $\tau_m < \tau_d$.

(iii) If the ratio τ_a/τ_d can be calculated or neglected.

2.2. Magnetic field pitch angle extraction from time delay estimations

According to equations (5) and (8), for a given separation (Δx and Δy) the time delay τ_m is a function of the perpendicular velocity $v_\perp$, the magnetic field pitch angle α and the ratio τ_a/τ_d. The value of α depends on the current profile in the plasma and is not known a priori, which makes the $v_\perp$ measurements more complicated. However, applying a three-point correlation technique with different poloidal and toroidal separations or multi-point measurements, α and $v_\perp$ can be determined simultaneously. Moreover, the ratio of two time delays from two different separations does not depend on $v_\perp$ so α can be determined as

$$\begin{aligned} \frac{\tau_{mi}}{\tau_{mj}} = \xi &= \frac{\Delta y_i + \Delta x_i \cdot \tan(\alpha)}{\Delta y_j + \Delta x_j \cdot \tan(\alpha)}, \\ \tan(\alpha) &= -\frac{\Delta y_i - \xi \cdot \Delta y_j}{\Delta x_i - \xi \cdot \Delta x_j}. \end{aligned} \tag{10}$$

Note that because the ratio does not depend on $v_\perp$, the α estimation is therefore not sensitive to the decorrelation time τ_d, as mentioned in section 2.1. The α is a non-linear function of the ratio ξ of two time delays. Using $\tan(\alpha) \approx \alpha$ for small angles we can approximate the errors in the α measurements as

$$\begin{aligned} \sigma_\alpha &= \sqrt{\left(\frac{\mathrm{d}\alpha}{\mathrm{d}\tau_{mi}} \cdot \sigma_{\tau_{mi}}\right)^2 + \left(\frac{\mathrm{d}\alpha}{\mathrm{d}\tau_{mj}} \cdot \sigma_{\tau_{mj}}\right)^2} \\ &= \sqrt{2}\frac{\sigma_{\tau_m}}{\tau_m}\frac{\Delta x_i \Delta y_j - \Delta y_i \Delta x_j}{(\Delta x_i - \xi \Delta x_j)^2}\xi. \end{aligned} \tag{11}$$

Here σ_{τ_m}/τ_m is the uncertainty in the time delay given in percent. The error in α depends on the time delay ratio ξ. Substituting ξ from equation 10 we obtain

$$\sigma_\alpha = \sqrt{2}\frac{\sigma_{\tau_m}}{\tau_m}\frac{(\Delta y_i + \Delta x_i \alpha)\,(\Delta y_j + \Delta x_j \alpha)}{(\Delta y_i \Delta x_j - \Delta x_i \Delta y_j)}. \tag{12}$$

Best resolution is achieved when one combination is aligned with the magnetic field line and another is perpendicular to it. An interesting case is obtained when $\Delta x_i = -\Delta x_j = \Delta y_i = \Delta y_j$. For this case we obtain

$$\sigma_\alpha = \frac{\sqrt{2}}{2}\frac{\sigma_{\tau_m}}{\tau_m}(1-\alpha^2). \tag{13}$$

For a 5 % error in the time delay measurements we obtain about a 2° error (worst case) in the measurement of the angle, which still allows for a realistic reconstruction of the α profiles. However, the α error can be reduced further if more than 2 time delay measurements are available, as is demonstrated in section 3.

2.3. Bayesian inference for multi-point time-delay measurements

Using multi-point measurements of fluctuations with N measurements permits the estimation of $M = N(N-1)/2$ different time delays. Ratios of time delays, with different poloidal Δy and toroidal Δx separations can be used for the estimation of α. However, to minimize the error we propose using a multi-point analysis of all possible measurement pairs with a Bayesian approach instead of using just the ratio of 2 time delays alone. The main benefit of this method is the ability to obtain an estimation of the probability to have a specific α and a specific $v_\perp$ from the M measured time delays. It is assumed that the measured time delays follow a normal distribution with mean τ_m, and variance σ_{τ_m}. The variance can be evaluated from successive measurements of the time delay for any combination. The Bayesian probability to obtain a specific α and a specific $v_\perp$ from M time delays is defined as

$$P(v_\perp, \alpha|\tau_{mi}, \sigma_{\tau_{mi}}) = \prod_{i=1}^{M} \frac{P(\tau_{mi}, \sigma_{\tau_{mi}}|v_\perp, \alpha)\cdot p(v_\perp, \alpha)}{p(\tau_{mi}, \sigma_{\tau_{mi}})}. \tag{14}$$

The prior probability $p(v_\perp, \alpha)$ is assumed equally distributed over some range of velocities and angles. The probability of the measurement $p(\tau_{mi}, \sigma_{\tau_{mi}})$ does not depend on $v_\perp$ and α and therefore can be used as a normalization factor. The likelihood $P(\tau_{mi}, \sigma_{\tau_{mi}}|v_\perp, \alpha) = \exp(-(\tau_{mi}-\tau(v_\perp, \alpha))^2/\sigma_{\tau^2_{mi}})$ describes the probability to measure a time delay τ_i if the real velocity is $v_\perp$ and the real pitch angle is α. The analytic function $\tau(v_\perp, \alpha)$ is obtained from geometry using equations (5) and (8), however, neglecting the factor τ_a/τ_d. The correction $(1-\tau_a^2/\tau_d^2)$ is taken into account after the Bayesian probability calculation. Error bars of measured pitch angles and velocities are estimated from the $1/e$ probability level in the $v_\perp$ and α accordingly.

2.4. Limitation of the method and declination of turbulent structures from the magnetic field line

In reality the turbulent structures are not perfectly aligned with the magnetic field lines but may have an additional inclination angle with respect to $\vec{B}$ due to a finite value

of the turbulence parallel correlation length $l_{||}$. The parallel correlation length can be estimated roughly by [18]

$$l_{||} = \frac{2\pi q_s R}{m - n q_s}, \tag{15}$$

where m and n are the poloidal and toroidal mode numbers of the turbulent structures and $q_s = (rB_t)/(RB_p)$ is the local safety factor. This equation can be rewritten using the local pitch angle $\tan(\alpha) = r/(Rq_s)$ and the inclination angle of the turbulent structure $\tan(\beta) = (rn)/(Rm)$

$$\tan(\beta) = \tan(\alpha) + \frac{2\pi}{l_{||} k_\theta}. \tag{16}$$

Here we introduce a poloidal wavenumber of the turbulent structures as $k_\theta = m/r$. This equation defines the declination of the turbulent structures from a magnetic field line. The equation coincides with one obtained by Mahdizadeh [16]. For the case of $k_\theta \rho_s \approx k_\perp \rho_s = 0.3$, as is suggested for TEM and ITG turbulence [19], a further dependence of α on the parallel correlation length (figure 3) is obtained.

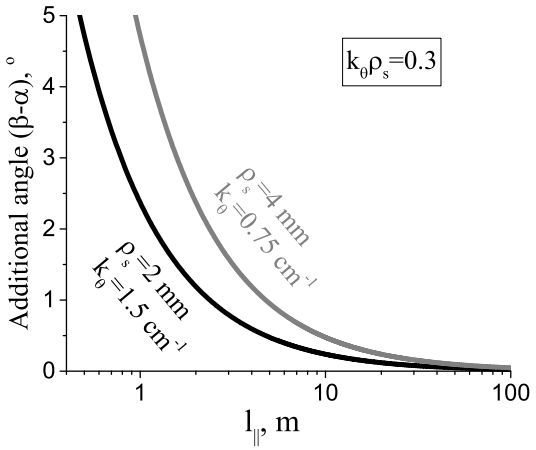

Figure 3. Inclination of turbulent structures versus parallel correlation length. The 2 different angles 5° and 10° and 2 different ρ_s value considered.

If $l_{||} > 10$ m, the declination is expected to be $< 1°$. Only a few publications report on measurements of parallel correlation length [14, 15, 16, 17] with values between 4 and 40 m reported. Recent parallel correlation length measurements from the TEXTOR tokamak give values between 11 and 22 m [20] indicating that the effect of structure declination is small. Conversely, if the real magnetic field pitch angle can be determined independently (i.e. MSE and/or magnetic equilibrium reconstruction) then the turbulence parallel correlation length could be obtained according to equation 16.

3. Poloidal correlation reflectometry

Any set of multi-point measurements of density or temperature fluctuations can be used for the reconstruction of the α and $v_\perp$ profiles from the correlation time delays. However, the requirement of high temporal (μs) and spatial (mm) resolution, restricts the number of possible diagnostics. Langmuir probes can be used, but they are generally limited to the cold plasma edge region. Laser based diagnostics are usually operated in a burst mode with low repetition rate. Microwave based diagnostics are good candidates with their high temporal and spatial resolution. In this section the

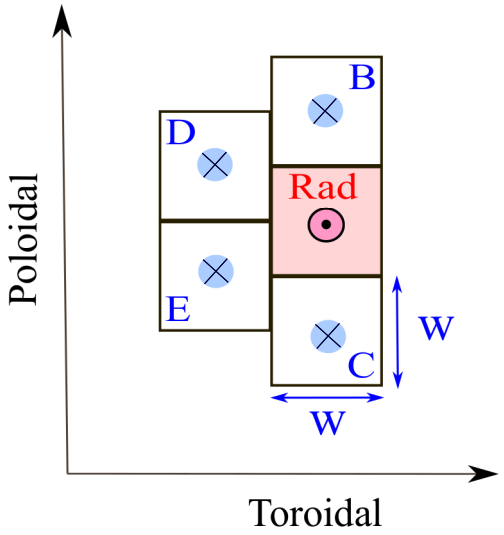

Figure 4. Schematic of PCR antennas array on ASDEX Upgrade. Rad (red) is transmitting while B,D,E,C (blue) are receiving antennas.

Poloidal Correlation Reflectometry (PCR) diagnostic is introduced for the time delay measurements of density fluctuations. The PCR launches a microwave beam into the plasma (perpendicular to the flux surfaces and parallel to the density gradient) where it propagates until it reaches a cutoff condition (where the plasma refractive index goes to zero) and is reflected. The reflected beam is measured by a cluster of several adjacent receiving antennas (figure 4 and 8), distributed poloidally and toroidally with respect to the launching antenna. Variations in the phase of the reflected microwave beams are related to movements in the density cutoff iso-layers, from which density fluctuations can be estimated [21].

By cross-correlating the reflectometer signals from arbitrary antennas pairs properties of the density fluctuation, such as the correlation length ($l_\perp$), decorrelation time (τ_d) and the fluctuation propagation velocity ($v_\perp$) can be obtained [22, 23, 24, 25, 26], and in addition the field-line pitch angle [27].

3.1. Pitch angle error for different antennas configuration

The number of receiving antennas is an important parameter for the velocity $\sigma_{v_\perp}$ and pitch angle σ_α errors. Using the Bayesian approach from section 2.3 with a

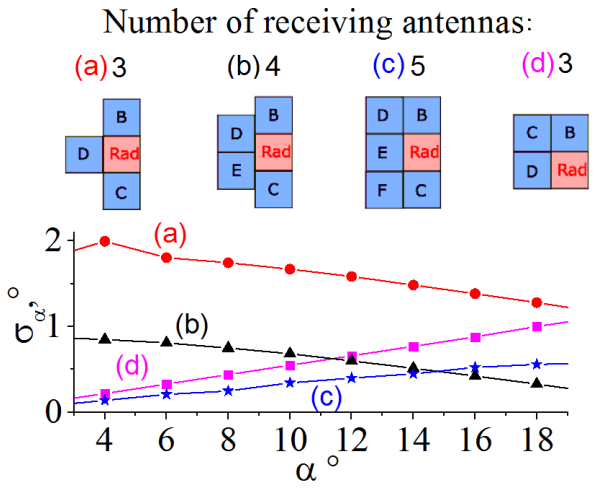

Figure 5. Error bars of α caused by uncertainties of time-delays $\sigma_{\tau_m}/\tau_m = 5\%$ for different antennas layouts. Red is emitting antenna and blue are receiving antennas.

5% uncertainty in the time delay, the pitch angle error σ_α can be calculated for different configurations of PCR antennas. Figure 5 shows 4 possible combination layouts with the respective an error σ_α as function of α. Only bistatic configurations are considered, where radiating antenna (red) is separated from receiving antennas (blue). If a monostatic system is used the number of antennas can be reduced by one. The σ_α of combination (a) is close to the result obtained by the analytic formula of equation 13. σ_α decreases with increasing number of receiving antennas. It is important to point out that not only the number of antennas but also their distribution is important for the minimization of σ_α. For example, at small angles ($\alpha < 10°$) configuration (d) offers better resolution with 3 receiving antennas than configuration (b) with 4 receiving antennas. Hence the design of the antenna cluster should be optimized for a particular tokamak. In this work configuration (b) is used for both TEXTOR and ASDEX Upgrade tokamaks.

3.2. Poloidal correlation reflectometry on TEXTOR

A PCR diagnostic was developed and used on the (now defunct) TEXTOR tokamak [23]. TEXTOR was a medium sized limiter tokamak ($R_o = 1.75$ m) with a circular plasma cross section ($a = 0.46$ m). The PCR diagnostic had a restricted probing frequency range covering the Ka band (27–37 GHz) corresponding to local densities of $0.9 - 1.7 \times 10^{19}$ m^{-3} in O-mode polarization. Two antenna arrays were operated (each with one launcher and four receiving antenna): one array pointing inwards from the tokamak low field side (LFS) mid-plane and one array pointing downward from

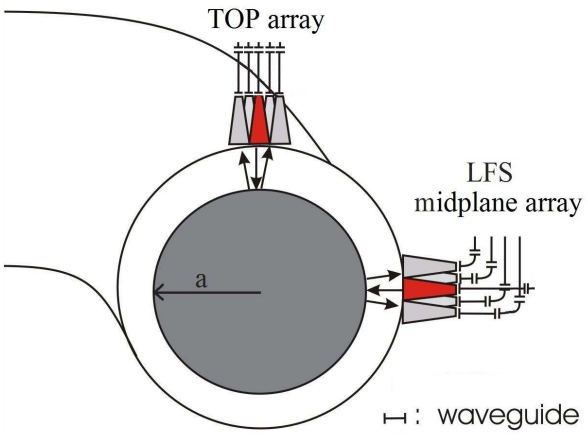

Figure 6. Schematic TEXTOR PCR front-end showing two arrays at the TOP and LFS midplane. Red is emitting antenna, grey are receiving antennas.

the vessel top at the plasma major radius R_o. The transmitting microwave generator and the heterodyne receivers were connected to the antennas by fundamental Ka-band waveguide. The microwave oscillator could be switched to any antenna combination in the top and LFS arrays. The antenna arrangement is shown in figure 6. The top array used rectangular antennas of 19×39 mm^2 while the LFS array used circular antennas with a diameter of 50 mm. The poloidal angle of the different combinations was $\theta = (0.025, 0.05, 0.075, 0.1)$ radian for the LFS and top arrays.
The launched beam and the receiver reference beam (with a 20 MHz offset) are generated by a YIG oscillator with low phase noise [24]. The reflected and the reference beams are combined in fundamental mixers followed by I/Q detectors. The resulting I and Q output signals are recorded with 14 bit resolution using INCAA data loggers at 1 MHz (later updated to 2 MHz).
The position of the reflection/cutoff layer is obtained using density profiles measured with a 9 channel HCN interferometer. From the line averaged data, density profiles have been calculated by Abel inversion every 10 ms. The density profiles are assumed to be symmetric in poloidal and toroidal direction, i.e. constant n_e on a flux surface.

3.3. Poloidal correlation reflectometry on ASDEX Upgrade

After the shut-down of TEXTOR the PCR system was transferred and installed on ASDEX Upgrade (AUG) [25]. AUG is a divertor tokamak with a D-shaped plasma cross section. Its major radius $R_0 = 1.65$ m is similar to that of TEXTOR, however, the range in plasma parameters and operation scenarios exceeds those of TEXTOR. A newly designed 5 antenna array with square aperture horns of 50×50 mm^2 allow both O-mode and X-mode polarization. Figure 4 shows a schematic of the antennas array, which is mounted on the LFS vessel mid-plane (figure 8) and focused to the magnetic axis. Due to limited space the connecting waveguide path is complicated and has a total length of about 10 m. The inner dimension of the waveguide is 10×10 mm^2 to allow

for both O-mode and X-mode propagation.
The heterodyne PCR system at AUG currently operates over both the Ka band (26–38 GHz) and (recently upgraded) U band (40–57 GHz). This entire frequency range corresponds to a local density range of 0.9–4×10^{19} m^{-3} in O-mode. The scheme of one U-band channel (emitting and one receiving channel) is shown in figure 7. A new dual-channel low noise (−150 dBc/Hz wide-band noise) microwave synthesizer in the range of 10–15 GHz is used for transmitter and local oscillator (LO) sources. The synthesizer works in fast frequency stepping mode with a transient switching time of < 60 μs. For heterodyne detection, transmitter and LO have a fixed frequency difference of 5 MHz. Active multipliers (×4) and power amplifiers extend the frequencies up to the U-band range. The power of the launched microwave is about 100 mW across the band. The reflected signal is mixed with the local reference signal and down-converted to an intermediate frequency (IF) of 20 MHz, followed by low frequency amplifiers and I/Q-detection section. The I and Q signals are digitized using a 2 MHz serial IO (SIO) ADC with 12 bit resolution. This scheme is repeated 4 times for all receiving antennas. A similar scheme is used for the Ka band, but with a 3–5 GHz range for the microwave synthesizer prior to up-conversion to Ka-band [25]. During each plasma discharge both the Ka-band and U-band data are collected simultaneously.

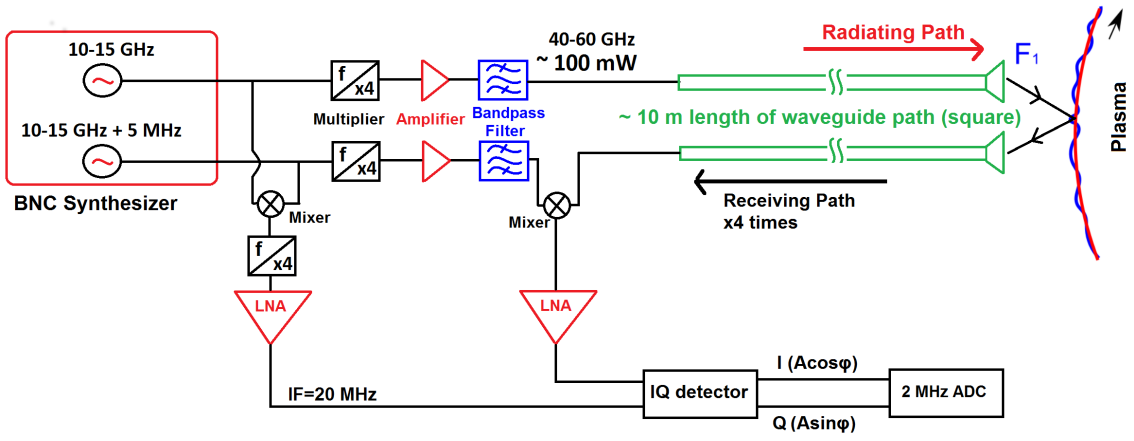

Figure 7. Scheme of one U-band channel (emitting and one receiving channel) of PCR on AUG.

In O-mode operation the measurement radial position depends on the density profile shape and on the line averaged density. For (low) core line averaged densities of $\bar{n}_0 \simeq 1.6 \times 10^{19}$ m^{-3} the system is capable of measuring density fluctuations from the plasma core to the edge (normalized poloidal flux radius $\rho_{\rm pol}$ =0.4–0.9). For higher densities ($\bar{n}_0 \simeq 4.7 \times 10^{19}$ m^{-3}) the edge region from $\rho_{\rm pol}$ =0.95–1.0 is covered only.

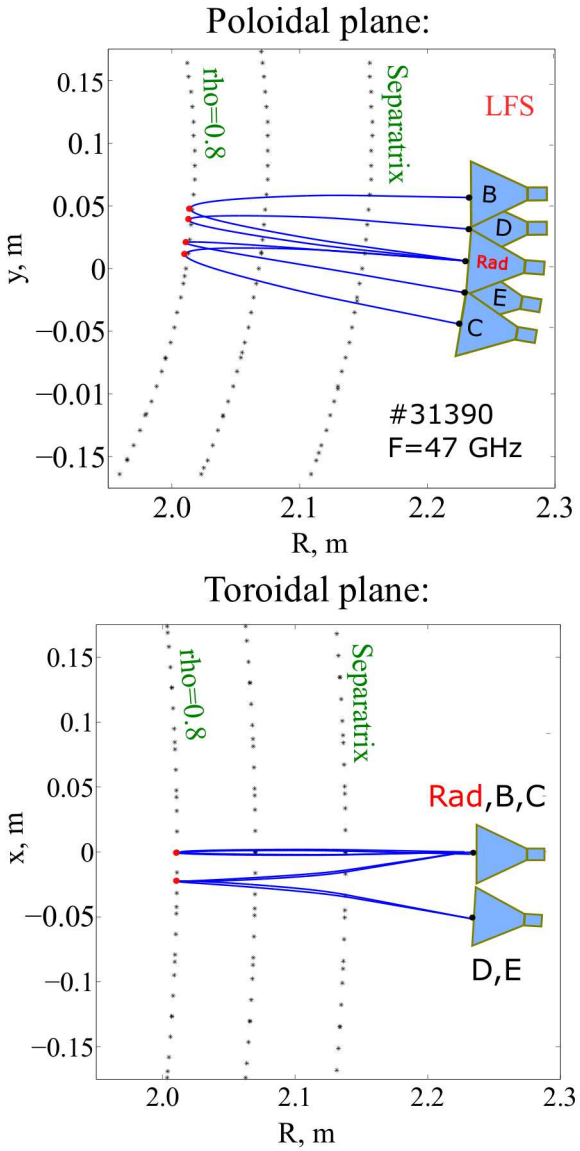

Figure 8. Examples of ray traces - starting from the launch antenna (Rad), propagate to the reflection/cutoff layer and then to the receiving antennas (B,C,D,E). Red points correspond to the reflection point.

3.4. Position of measurements and beam tracing code TorBeam

To correlate signals from poloidally and toroidally separated antennas, the precise position of the reflection points needs to be known. The poloidal and toroidal measurement positions are not a fixed function of the radius, but depend on the cutoff layer curvature (poloidal R_{pol} and toroidal R_{tor}) and the shape of the magnetic surface (e.g. vertical and horizontal shift of the plasma column). Additionally, the measurement position could be affected by refraction during the propagation of microwave beam, especially when gradients in the refractive index become small.

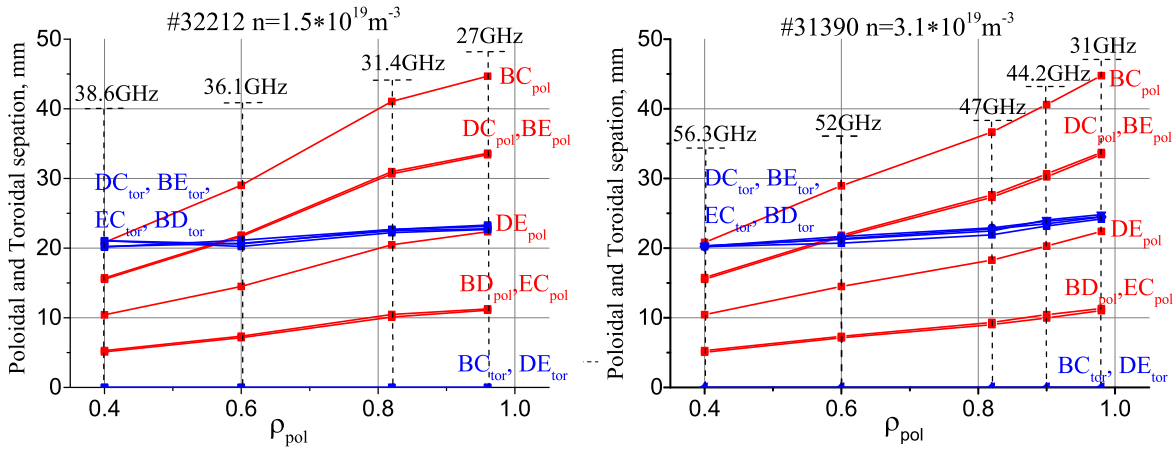

Figure 9. Comparison of poloidal and toroidal separation between the measurement points of different horns antennas (B,C,D,E) for two shots with different densities. To have the same reflection layer the launch frequency was changed.

At TEXTOR a simple calculation based on a circular poloidal cross-section of the iso-density surface was sufficient to obtain the reflection positions [24]. However, the D-shape poloidal cross-section of AUG requires a more sophisticated approach. Here, the beam tracing code TORBEAM [28] is used with the real geometry of AUG plasmas and antennas, together with fitted electron density profiles and magnetic equilibria from the CLISTE code. The radiation patterns of the launch/receiving antennas have a sufficiently wide beam width (spot overlap) that an optimal ray exists that passes from the centre of the launch antenna orifice to each of the receive antennas. The half power beam width $\Delta\theta_{3dB}$ is varies from 13° at 26 GHz to 7° at 57 GHz. The optimal ray (and hence reflection position) is found by tracing a set of rays with different angles within the launch radiation pattern.

Figure 8 shows examples of the ray-tracing calculations for the conditions of discharge #31390 and a probing frequency of $f = 47$ GHz. The turning points of the reflected rays (red bold points) define the measurement positions for each antenna pair. For the plasma edge region ($\rho_{\rm pol} \simeq 0.98$) and a typical plasma geometry the separation between points amounts to $\Delta y = (11.2, 22.0, 33.54, 44.5)$ mm in the poloidal direction and $\Delta x = (0, 23.1)$ mm in the toroidal direction.

The separations are investigated as function of different cutoff radii, different plasma densities and different magnetic configurations. In figure 9 the poloidal and toroidal separation for two discharges with different line averaged densities (lower single-null X-point, positive I_p and negative B_t) are shown. For the core line averaged density $\bar{n}_0 = 1.5 \times 10^{19}$ m^{-3}, (figure 9a), ray-tracing has been performed using frequencies from 27 GHz at $\rho_{\rm pol} = 0.96$ to 38.6 GHz at $\rho_{\rm pol} = 0.4$. A strong dependence of the poloidal separation with $\rho_{\rm pol}$ is observed, which can be explained by a large change in the poloidal curvature R_{pol}. However, the toroidal dependence is weak, due to a small change in the toroidal curvature R_{tor} across $\rho_{\rm pol}$ only. A comparison of separations at higher density

$\bar{n}_0 = 3.1 \times 10^{19}$ m^{-3}, shown in figure 9b, give similar results, despite the fact that the probing frequencies are different, starting from 31 GHz at $\rho_{\rm pol} = 0.98$ to 56.3 GHz at $\rho_{\rm pol} = 0.4$. This suggest that the effect of the frequency is small and that the main dependence comes from the curvature of the magnetic surfaces. In addition the effect of a vertical shift of the plasma is studied in the range of ± 25 mm. Only a very weak change in the poloidal and toroidal separations in the order of 2 % is found which does not exceed the measurement error of α. Based on these calculations we conclude, that despite the fact that the separation depends on the magnetic configuration, this does not influence substantially the α measurements. Thus the PCR method can be robustly used for pitch angle and perpendicular velocity measurements.

3.5. Radial resolution of measurements

The radial resolution of the PCR diagnostic has been approximated by the full-width at half-maximum of the first Airy lobe of the microwave electric field square E^2 at the cutoff layer. For O-mode polarization with moderate value of the density gradient scale length $L_n = |\frac{1}{n}\frac{dn}{dx}|^{-1}$ this is given by [29]

$$\delta R = \frac{1.6 L_n}{[(\omega/c) L_n]^{2/3}} \tag{17}$$

where $\omega = \omega_{pl}(n_e) = \sqrt{\frac{n_e e^2}{m_e \epsilon_0}}$ is estimated from the density profile at the reflection position.

The typical radial resolution is of the order of 2–12 mm depending on the density and probing frequency. It is interesting to note that the resolution improves at the edge due to decreasing L_n and reaches values in the range 2–4 mm. It has been reported that the radial resolution of the method can deteriorate due to small angle scattering of microwaves [30, 31].

4. Magnetic field pitch angle and perpendicular velocity studies at TEXTOR and AUG

The results presented in this section are obtained for L-mode discharges and O-mode polarization.

4.1. Time delay measurements and effect of pitch angle

Typically density fluctuation spectra are found to be similar for all receiving antennas [25, 26]. Analyzing the normalized CCF $\rho_{XY}(\tau)$ between two time series (X, Y) from different antennas yields the maximum correlation delay time τ_m as a function of the poloidal and toroidal separation

$$\tau_m = \arg\max_\tau(|\ \rho_{XY}(\tau)\ |) \tag{18}$$

where

$$\rho_{XY}(\tau) = \frac{\sum_i X(t_i) \cdot Y^{\star}(t_i + \tau)}{\sqrt{\sum_i X^2(t_i) \cdot \sum_i Y^2(t_i)}}. \tag{19}$$

Figure 10a depicts all possible CCFs for AUG shot #32843 at $t = 3.31$s within time windows of 5 ms. The position of measurement is $\rho_{pol} = 0.98$ at the LFS midplane. The maximum correlation time delay τ_m indeed varies with the antenna pair separation. Note that all CCFs can be fitted with a gaussian function $\rho_m \exp(-(\tau - \tau_m)^2/\tau_0^2)$. Not only the maximum correlation delay time, but also the maximum correlation level ρ_m varies with the antennas separation. The reason is the decorrelation of the turbulence during propagation in agreement with section 2.1. We can describe the decorrelation effect by an envelope $\rho_{env} \exp(-\tau^2/\tau_d^2)$ with the decorrelation time τ_d as shown for the presented case of 10.5 μs. This indicates that for the calculation of the perpendicular velocity the decorrelation time can be important (section 2.1), however, for the presented case the correction factor $(1 - \tau_a^2/\tau_d^2)$ only amounts to 0.94. This correction has been taken into account in the following analyses.

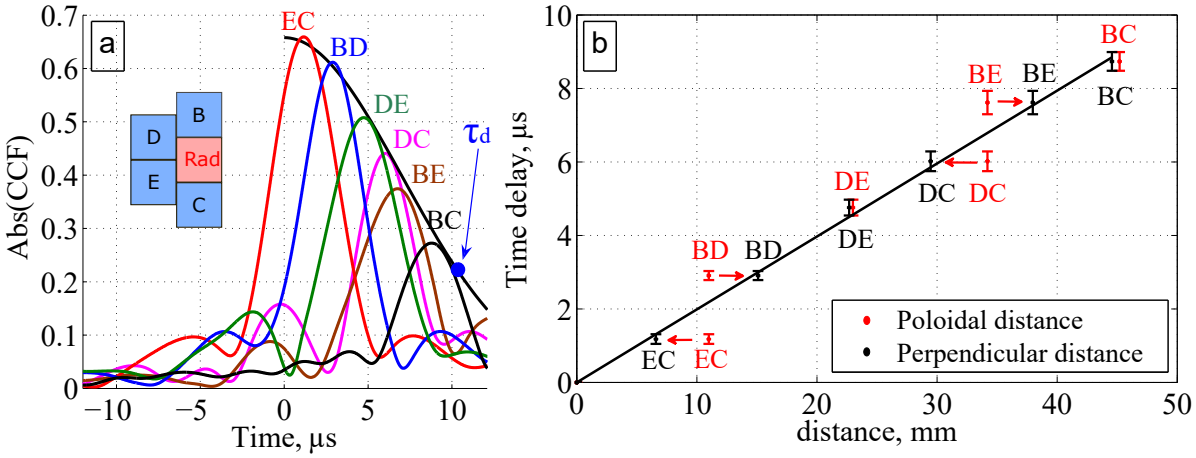

Figure 10. (a) Normalized cross-correlation for various antenna pair combinations. (b) Maximum correlation time delay as a function of poloidal Δy (red) and perpendicular distance $\varepsilon_\perp$ (black). The position of measurement is $\rho_{pol} = 0.98$ LFS midplane. The value of magnetic field pitch angle is 9.5°.

In figure 10b different τ_m are obtained for each antenna pair combination with different toroidal signs $\Delta x_i = -\Delta x_j$ but equal poloidal signs $\Delta y_i = \Delta y_j$. The reason for this difference has its origin in the pitch angle, as discussed in section 2.1. In figure 10b the τ_m values are shown as a function of the poloidal separation Δy (red points) and as a function of the perpendicular separation $\varepsilon_\perp$ (black points). Here $\varepsilon_\perp$ denotes the separation of the antennas perpendicular to $\vec{B}$ according to the equation 5. Assuming a constant perpendicular velocity $v_\perp$ the deviation from the linear regression fit (line) with the poloidal separation values (red) is due to an inclination angle. This angle is, to first order, the magnetic pitch angle. This deviation disappears by plotting time delay versus the perpendicular separation (black points), calculated using equation 5.

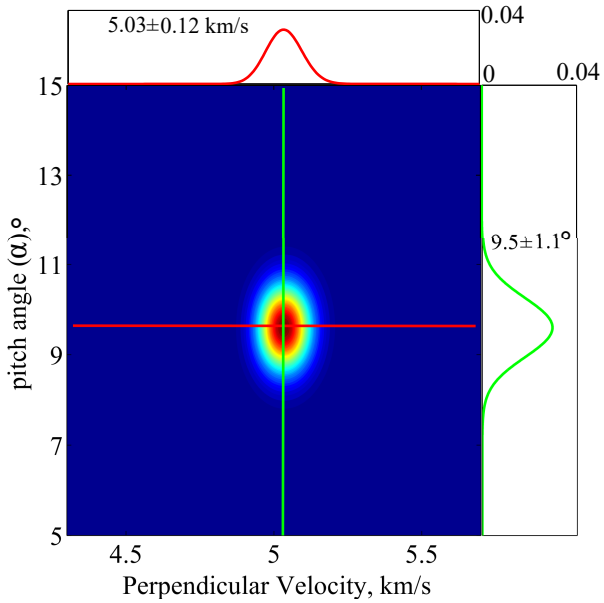

Figure 11. Bayesian probability function for shot #32843 of AUG. The position of measurement is $\rho_{pol} = 0.98$ LFS midplane.

A more accurate estimation of α and $v_\perp$ can be obtained using the Bayesian approach from section 2.3. The Bayesian probability for the same shot is shown in figure 11. The centre of gravity of the spot represents the most probable values for the pitch angle α and the perpendicular velocity $v_\perp$. Error bars of measured α and $v_\perp$ are estimated from the $1/e$ level of the probability function in the α and $v_\perp$ directions, accordingly.

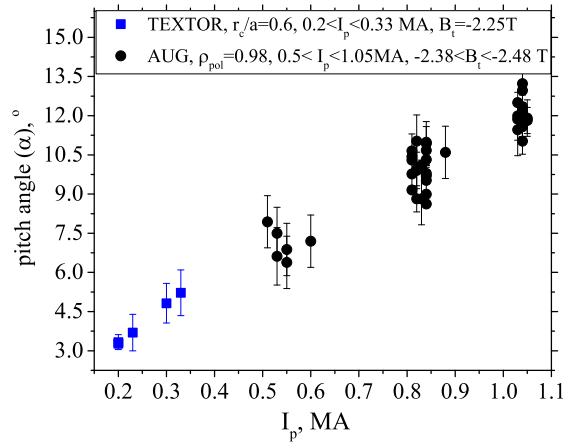

Figure 12. Variation of measured pitch angle for different plasma current at TEXTOR and AUG. The positions of measurement are LFS midpane for both devices.

Further studies on the dependence of α on the magnetic field B_t and plasma current I_p show the expected behaviour for both tokamaks. Inversion of α with inversion of either B_t or I_p is observed. An increase of α with I_p is observed as well. This is shown in figure 12 where α measured on both devices are plotted in the same figure. For this

data set a series of discharges was analysed for different I_p. At TEXTOR, $B_t = 2.25$ T and position $r_c/a = 0.6$ are used. At AUG the analysis is performed in edge region at $\rho_{\mathrm{pol}} = 0.98$. The B_t values for different shots have a small variation between 2.38 and 2.48 T. The position of the measurements are the LFS midpane for both devices. Independent of the machine parameters a rather good linear dependence is found. The dependence on the magnetic field has also been studied. Here, a decrease of α with increasing B_t is observed.

4.2. The perpendicular velocity profile from AUG and effect of decorrelation time

By scanning the frequency, radial profiles of $v_\perp$ from both tokamaks are obtained. An example of a $v_\perp$ profile obtained from AUG discharge #32294 is shown in figure 13a (red line). Here the Bayesian approach (section 2.3) has been applied to obtain $v_\perp$ and its

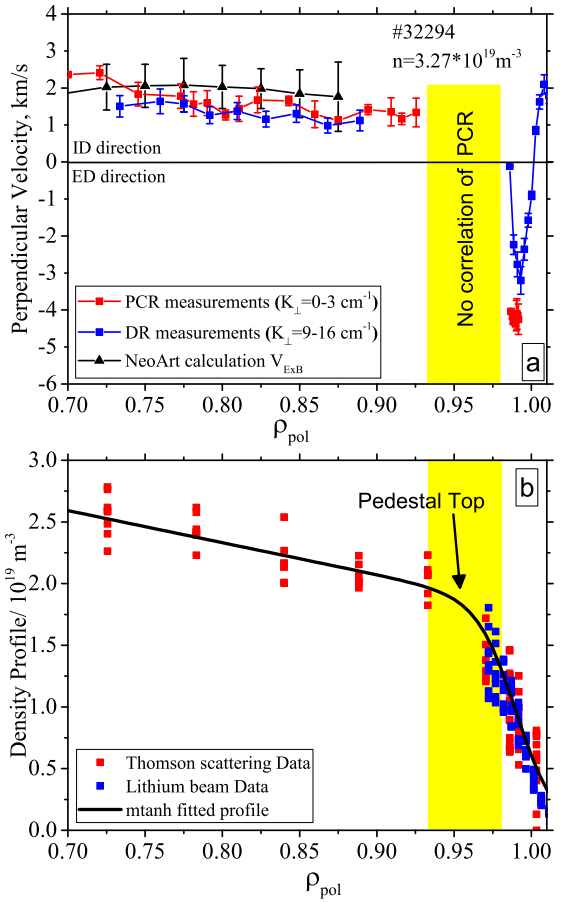

Figure 13. (a) Velocity profiles from shot #32294 of AUG. (b) Electron density profile from shot #32294. The position of measurement is LFS midplane.

error $\sigma_{v_\perp}$. All points additionally have been corrected with the decorrelation correction (section 2.1). The correction factor $(1 - \tau_a^2/\tau_d^2)$ was about of 0.94, except in the shear region where the correction factor was 0.8. The measurement of $v_\perp$ has been compared with Doppler Reflectometry (DR), which measures the local $v_\perp = v_{E\times B} + v_{ph}(k_\perp)$

from the Doppler shift of a backscattered signal from turbulent fluctuations at some specific wavelength $k_\perp$ [33, 32]. For comparison the DR measurements (blue curve) have been projected from their measurement location to the position of PCR (midplane) by correcting the radial electric field due to magnetic flux surface compression. It is important to emphasize that the DR measures at higher wavenumber $k_\perp = 9$–16 cm^{-1} compared to the PCR with $k_\perp = 0$–3cm^{-1}. A dependence of $v_\perp$ on the wavenumber $k_\perp$ could arises from a change in the turbulent phase velocity Δv_{ph}. The measured $v_\perp$ from PCR and DR yield similar values and the same trend (figure 13a). The difference at ($\rho_{\rm pol} = 0.7$–0.92) is small (< 0.3 km/s) and inside the error bar of the measurements. However, the difference in the edge ($\rho_{\rm pol} = 0.98$–1.00) of the order 0.5 km/s might be related to different phase velocities of the turbulence. More detailed profiles in the plasma edge region for shot #32316 are shown in figure 14a. A full scan of different

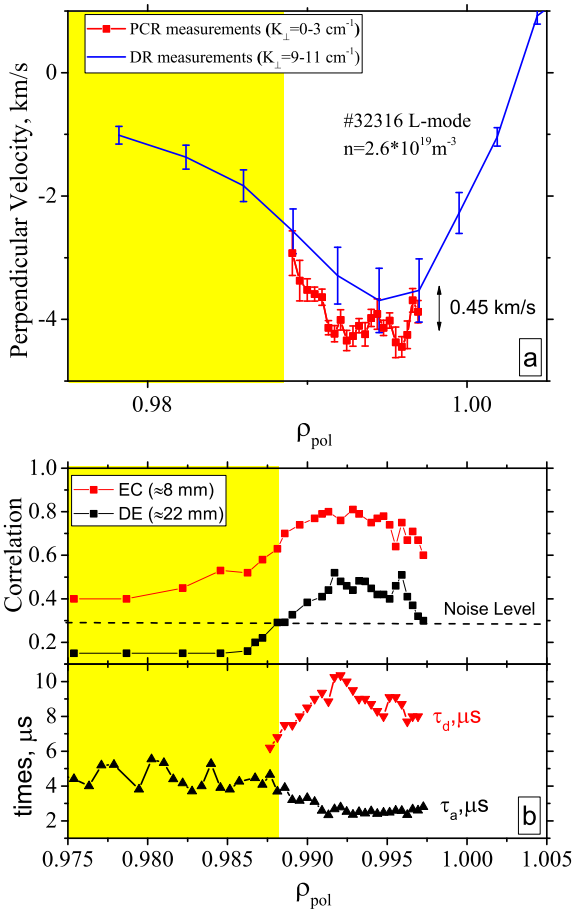

Figure 14. (a) zoom in velocity profiles of edge region #32316 of AUG. (b) Correlation level for 2 separations (8mm and 22mm), decorrelation time and autocorrelation time in the edge region of #32316. The position of measurement is LFS midplane.

$k_\perp$ in the edge region was performed using a Doppler Reflectometer with a movable mirror [33]. The results shown in figure 15 suggest that dependence of $v_{ph}(k_\perp)$ is small ($\Delta v_{ph} \approx 0.35$ km/s between $k_\perp = 0$–3 cm^{-1} and $k_\perp = 9$–11 cm^{-1}). The difference of

phase velocities in the edge is significantly lower, than suggested by linear drift wave theory ($\Delta v_{ph} \approx$ 3-5 km/s between $k_\perp = 1$ cm^{-1} and $k_\perp = 11$ cm^{-1}) calculated using $v_{ph}(k_\perp) = \rho_s c_s/(L_n(1 + k_\perp^2 \rho_s^2))$ [34] with drift wave scale $\rho_s = \sqrt{m_i T_e}/eB$ and sound speed $c_s = \sqrt{T_e/m_i}$.

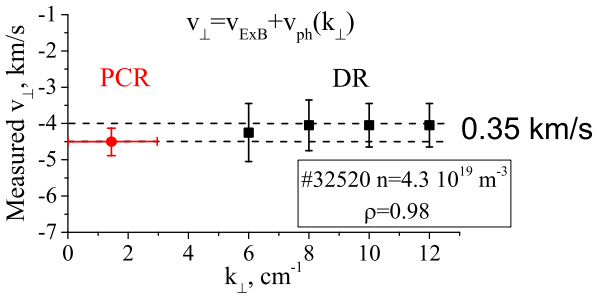

Figure 15. Comparison of measured velocity at different $k_\perp$ with doppler reflectometry ($k_\perp$=6, 8, 10, 12 cm^{-1}) and poloidal correlation reflectometry ($k_\perp$=0–3 cm^{-1}).

Since both PCR and DR measure similar velocities $v_\perp = v_{E\times B} + v_{ph}(k_\perp)$ (independent of $k_\perp$) it might be possible to estimate the magnitude of v_{ph} from the difference with neoclassic calculations of the $E \times B$ flow velocity $v_{E\times B}$ obtained from the NEOART code [35], which includes fluid toroidal rotation measurements from charge exchange recombination spectroscopy. The results over the range ρ_{pol}= 0.7–0.92 is shown in figure 13a (black triangles). Here the neoclassical $v_{E\times B}$ and the measured $v_\perp$ by PCR are very close again, and hence the phase velocity is smaller than the error bars of the NEOART calculations ($\approx$ 0.5 km/s). The NEOART code has been compared earlier with fluid velocity measurements from charge exchange recombination spectroscopy [36, 37] and shows good agreement. Unfortunately the neoclassical calculation at the plasma edge has big uncertainties for the present shot, related to the poor resolution of the gradient measurements.

It is important to note that the $v_\perp$ profile (red line in figure 13a) has a gap in the region $\rho_{\rm pol}$ = 0.92–0.985, which is related to a loss of correlation at these radii (although the fluctuation signal remains strong). The correlation level for two different separations (8 and 22 mm) is shown in figure 14b. A possible impact of probing frequencies can be excluded, since for different density profiles the loss of correlation is observed at different frequencies. The affected frequency range always corresponds to cutoff positions around the pedestal top (figure 13b). The small pedestal in the electron densities is a feature of X-point plasmas and is found even in L-mode. It should be noted that the position of correlation loss is inside of the negative shear flow (figure 14a).

A possible mechanism explaining the loss of correlation is a decrease of the decorrelation time τ_d in the shear region (figure 14b). For the small value of τ_d, eddies on the magnetic surface decorrelate faster than the time needed for the propagation between the measurement volumes. On the other hand, the autocorrelation time measurement τ_a shows an increase towards the shear region, due to the decrease of the velocity

according to equation 7. However, at the point where $\tau_a \approx \tau_d$ the autocorrelation time doesn't increase anymore and stays constant. This can be explained by the fact that the autocorrelation time (equation 7) is dominated by the decorrelation time of the turbulence. Doppler reflectometry of course does not lose the measurement capability (figure 14a), since it use only a single point for the measurement of the velocity. The results are shown for negative shear, however, additional similar observations have also been obtained in AUG (not shown here) for the positive shear.

4.3. The magnetic field pitch angle profile from TEXTOR

Pitch angle profiles have been measured in both tokamaks. Figure 16 shows an example profile obtained from the top (circles) and LFS (squares) antenna arrays of the TEXTOR tokamak. For this dataset plasmas with $B_t = 1.9\ T$ and different densities $\bar{n}_0 = [1, 1.5, 2.0]\times10^{19}$ m^{-3} have been investigated. During the discharge a current ramp from 400 down to 250 kA has been carried out. The LFS and top measurement yield similar pitch angle values at r_c/a =0.8 independent of the position of antenna array (i.e. helicity is constant). Although note that the values of the pitch angle measured with the LFS antennas at r_c/a =0.7 are slightly higher. This may be linked with magnetic compression on the LFS due to Shafranov shift.

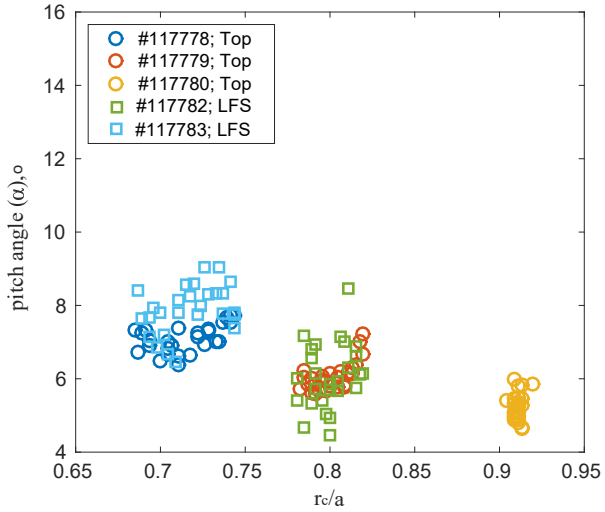

Figure 16. Scaling of α with r_c/a from top (circles) and LFS (squares) antennas arrays position at TEXTOR.

For TEXTOR, with its circular plasma shape, the local q profile has been estimated from α using the following equation for top antennas array

$$q_{\mathrm{TOP}}(r) = \frac{r}{R_0 \tan(\alpha)}. \tag{20}$$

Here the minor radius of the plasma is denoted by r, and the major radius of plasma $R_0 = 1.75$ m is used. Note that this equation is not applicable for the AUG tokamak due to the non-circular plasma cross-section. In figure 17 the evolution of the q_{TOP}

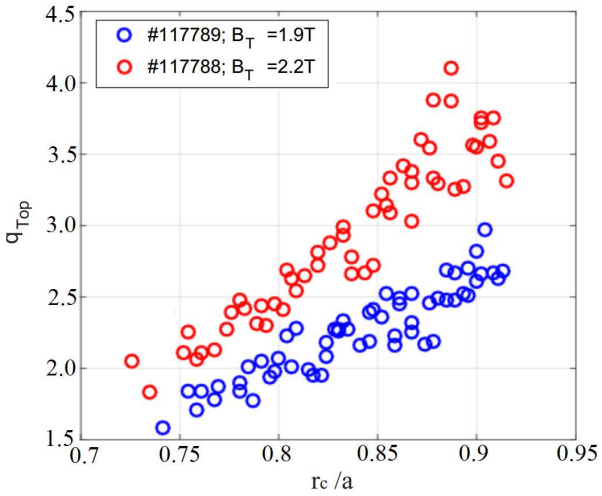

Figure 17. Estimation of $|q|$ from top antennas array at TEXTOR for two values of toroidal magnetic field.

profile with respect to the reflection layer and for 2 different magnetic field strength is shown (top antennas array, #117788-89). The data are achieved by applying a density ramp $\bar{n}_0$ from 1.5 to 3.0 $\times$ 10^{19} m^{-3} at fixed probing frequency. As expected the q_{TOP} value for $B_t = 1.9$ T are lower than for $B_t = 2.2$ T. This becomes especially clear in the plasma edge where q is higher. All observations confirm that the measured angle is closely linked to the magnetic field line pitch angle. It is interesting to note that around rational surface locations ($q = 2/1, 5/2, 3/1$) the q_{TOP} profile appears to show dips, which may be related to magnetic island formation. However, further studies are needed and are outside of the scope of the present paper.

4.4. Comparison with the CLISTE *code at AUG*

For AUG, α measurements have been contrasted with magnetic equilibrium reconstructions from the CLISTE code [38]. Here, the α profile from the CLISTE is computed directly from the magnetic field components (B_R, B_z, B_ϕ) from the equilibrium reconstruction at the corresponding PCR measurement location

$$\alpha = \arctan\left(\frac{B_\theta}{B_\phi}\right) = \arctan\left(\frac{\sqrt{B_R^2 + B_z^2}}{B_\phi}\right). \tag{21}$$

For typical L-mode plasmas the α profile from the CLISTE reconstruction over the range ρ_{pol} =0.7–1.0 is almost flat. Both the α profile (using Bayesian analysis) and the parametric dependence of α at fixed radius from different shots have been compared. Figures 18 and 19 depict results of comparison from the edge ρ_{pol} =0.97–0.99 and the core ρ_{pol} =0.7–0.94 regions.

Figure 18a shows a comparison of the PCR calculated α with equilibrium values in the plasma edge at ρ_{pol} =0.97–0.99 for 20 shots. Good similarity is observed, with a

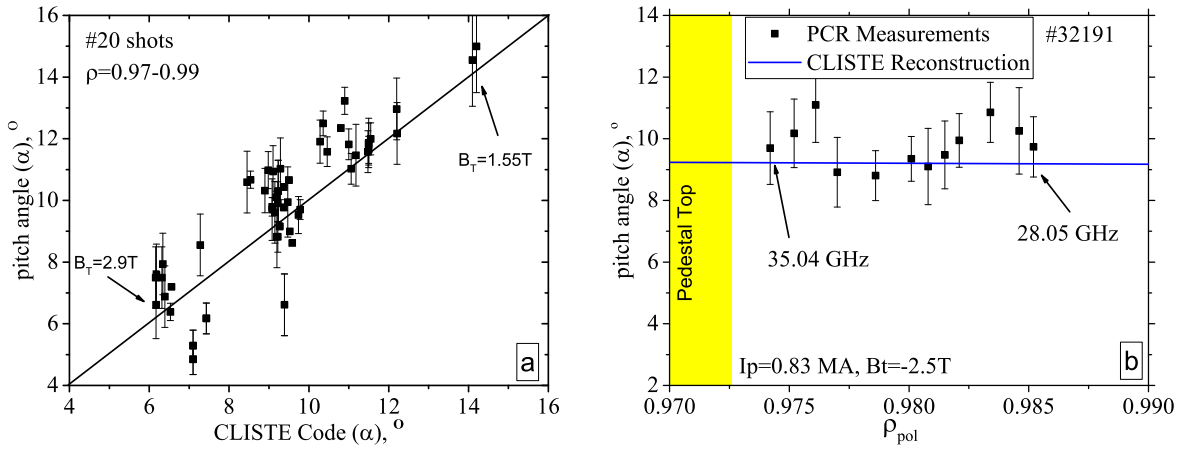

Figure 18. (a) Comparison of α measured by PCR with reconstructed values from CLISTE equilibrium code. 20 different shots at AUG have been compared in edge region. (b) Profile of α in edge region of plasma. The position of measurements are LFS midplane.

few notable outliers. For each shot a plasma phase ($\simeq$20 ms long) was selected with stable plasma plasma parameters in terms of plasma current, magnetic field and density. Across the database B_t varied between 1.55 and 2.9 T and I_p between 0.5 and 1.05 MA. To minimize the effect of the density profile, only shots with averaged line densities in the range n_0 =2.5–3.2$\times 10^{19}$ m^{-3} were used. This constraint ensures (i) the same radial resolution for the measurement and (ii) the same poloidal and toroidal separation between measured time delays. The discharges in figure 18a with significant deviations between measured and equilibrium α cannot be explained by the measurement error bars alone. Indeed, during individual shots with the constant radial position the measured difference between PCR and CLISTE remains constant. The pitch angle profile at the edge in figure 18b shows similar values for all probing frequencies across the plasma edge region, which are in good agreement with the CLISTE. This demonstrates that the method gives the same results independent of the probing frequency used. It is interesting to note that the profile shows weak wavelike radial structure. This structure can explain the spread of points in figure 18a.

Figure 19a shows a comparison of PCR and CLISTE pitch angles for the core plasma region $\rho_{\rm pol}$ =0.7–0.94 of shot #32212. Two frequency sweeps were made during a stable flat density phase and both profiles show a similar shape. Deviations from the constant CLISTE value are found at $\rho_{\rm pol}$=0.90–0.95 (left of the density pedestal position) reaching values of 2–3°. However, this deviation decreases, when going deeper in the core. Similar observations are obtained when using a density scan with a fixed probing frequency instead of a frequency scan with fixed density, as shown for shot #31427 in figure 19b. In the following, different effects are discussed which could be cause for the discrepancy.

(i) In order to increase the calculated pitch angle by CLISTE, the current density around the pedestal position would need to be increased. To get agreement between PCR

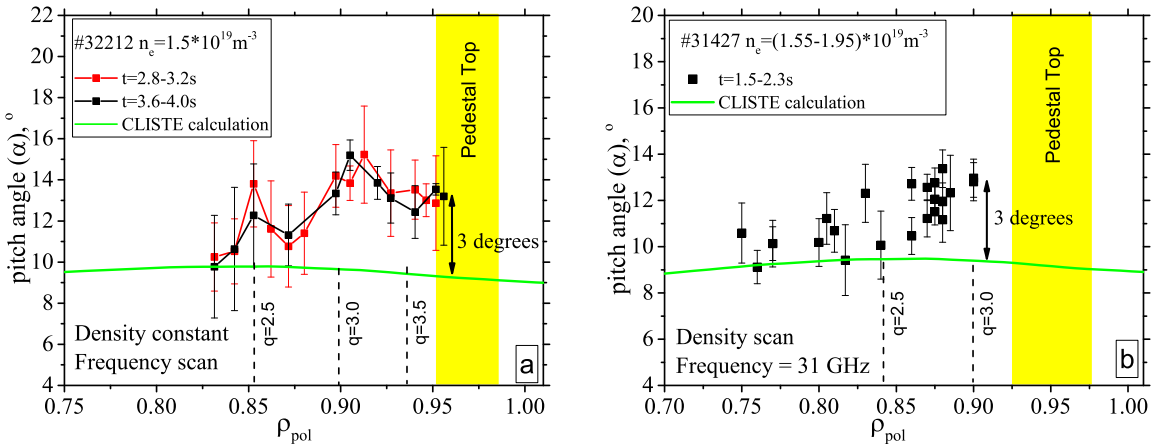

Figure 19. Comparison of α profile for core region of plasma: (a) from 2 Ka-band frequency sweeps with constant density and (b) during density ramp with fixed probing frequency. The position of measurements are LFS midplane.

and CLISTE the integral current $\int j(r)dr$ would need to be increased by 150–200 kA. This change is unrealistically large compared to the total plasma current of 800 kA. The effect of the edge bootstrap current was evaluated to be $< 0.25°$.

(ii) The difference between PCR and CLISTE could appear because CLISTE produces an axisymmetric reconstruction, while the PCR angle measurements are (toroidally) local. The toroidal magnetic field ripple effect can create a difference. If this was the reason local PCR angles might be used as an additional parameter for a better 3D equilibrium reconstruction. However, calculations by Strumberger [41] suggest that magnetic field ripple effect is small(<1%) and can not explain the difference.

(iii) The measured angle is a superposition of the magnetic field pitch angle and an additional turbulence inclination angle (section 2.4). To obtain a 2–3° declination for turbulent structures with $k_\perp \rho_s = 0.3$ a parallel correlation length of 2 m is necessary. The decrease of the difference in α towards the core could be due to an increase in parallel correlation length according to equation 16. A parallel correlation length of 2 m would be rather small compared to result from previous studies [14, 15, 16, 17](but not impossible).

(iv) The wavelike structure in the radial pitch angle profile can be a signature of small islands around rational surfaces. In the radial region shown in figure 19a the rational surfaces $q = 2/1,\ 5/2,\ 3/1$ are located according to the CLISTE code. An small oscillation in the pitch angle are also observed in the TEXTOR results (figure 17).

It is important to note that the pitch angle measurement at the edge ($\rho_{\rm pol} = 0.98$) has been additionally validated using the long range correlation (LRC) between two independent reflectometer systems at AUG: the O-mode PCR located in toroidal sector 2, and secondly an O-mode, dual-channel (Q & V-band) frequency-hopping reflectometer system in toroidal sector 5 [39, 40]. The separation between systems amounts to 1.5 m and 0.12 m in toroidal and poloidal direction, respectively. A high correlation (≈20%)

is measured if the 2 systems are on the same flux surface (there is a frequency overlap between the Ka and Q-bands) and close to a connection by a magnetic field line, which can be varied by the edge q-profile. This method has been used to calculate the pitch angle showing consistent results.

5. Conclusions

We have demonstrated that poloidal correlation reflectometry is a valuable tool for the localized measurement of the magnetic field pitch angle α and the perpendicular plasma velocity $v_\perp$ profiles. The method is based on the measurement of time delays of propagating plasma density fluctuations from poloidally and toroidally separated antennas, assuming that the fluctuations are aligned with the magnetic field line. A Bayesian approach has been developed and applied for the reconstruction of α and $v_\perp$ profiles from the measured maximum correlation time delays. Results are presented from the tokamaks TEXTOR and ASDEX Upgrade with L-mode plasmas.
The perpendicular velocity profile obtained with PCR at AUG shows good agreement with neoclassical fluid velocities from the NEOART code and with measurements from Doppler reflectometry in the core. However, small difference of the order of 0.5 km/s (electron diamagnetic direction) between PCR ($k_\perp \approx 1\ cm^{-1}$) and DR ($k_\perp \approx 11\ cm^{-1}$) observed in the edge, which may be connected to a difference in phase velocities Δv_{ph}. The difference Δv_{ph} is significantly smaller than predicted for linear drift waves ($\Delta v_{ph} \approx$ 3–5 km/s between $k_\perp = 1$ cm^{-1} and $k_\perp = 11$ cm^{-1}). It is found that around the edge E_r shear layer the decorrelation time τ_d of turbulence is reduced, making $v_\perp$ measurements at these radii difficult.
The magnetic field pitch angle has been measured as a function of B_t and I_p and the expected dependencies have been observed. Similar profiles from the top and LFS launch in TEXTOR have been obtained. The calculation of local q profiles from the pitch angle profiles also yields reasonable results. A comparison with the equilibrium reconstruction code CLISTE at AUG shows similar values in the core and edge. However, a difference of the order of 2–3 $^\circ$ remains at the density pedestal position. A possible explanation for the deviation is a small value for the parallel fluctuation correlation length. For the considered plasma condition at pedestal position and $k_\perp \rho_s = 0.3$ a parallel correlation length of $\approx$ 2 m would be needed to reconstitute the experimental with equilibrium calculations. The decrease of the α difference towards the core and edge could be due to an increase in parallel correlation length according to equation 16.
As a result of these studies we conclude that the magnetic field pitch angle and perpendicular velocity can be measured from the inclination of turbulent structures with PCR. The impact of a measured declination of turbulent structures from the magnetic field line could be the reason for deviation of a few degree in α. In future work studies of pitch angle dynamics during the development of MHD instabilities are foreseen.

Acknowledgments

We thank J. Friesen and D. Grossman for assistance with hardware construction. E. Poli, M. Dunne, G. Birkenmeier and P. Hennequin for fruitful discussions.
This work has been carried out within the framework of the EUROfusion Consortium and has received funding from the Euratom research and training programme 2014-2018 under grant agreement No 633053. The views and opinions expressed herein do not necessarily reflect those of the European Commission. This work was also performed within the framework of the Helmholtz Virtual Institute on Plasma Dynamical Processes and Turbulence Studies using Advanced Microwave Diagnostics.

References

[1] Sauter O, Angioni C and Lin-Liu Y R 1999 "Neoclassical conductivity and bootstrap current formulas for general axisymmetric equilibria and arbitrary collisionality regime", *Phys. of Plasmas* **6** 2834
[2] Wolf R C 2002 "Internal transport barriers in tokamak plasmas", *Plasma Phys. Control. Fusion* **45** R1-R91
[3] Buttery R J, Gunter S, Giruzzi G, Hendert T C, Howell D, Huysmans G, La Haye R J, Maraschek M, Reimerdes H, Sauter O, Warrick C D, Wilson H R, Zohm H 2000 "Neoclassical tearing modes", *Plasma Phys. Control. Fusion* **42** B61-B73
[4] Snyder P B 2002 "Edge localized modes and the pedestal: A model based on coupled peeling–ballooning modes", *Phys. Plasmas* **9** 2037
[5] Howard J 1999 "Optical coherence-based techniques for motional stark effect measurements of magnetic field pitch angle", *Plasma Phys. Control. Fusion* **41** 271
[6] Soltwisch H 1986, "Current distribution measurement in a tokamak by FIR polarimetry", *Rev. Sci. Instrum.* **57** 1939–1944
[7] Holloway C.L, Doviak R.J, Cohn S.A, Lataitis R.J, Van Baelen J.S 1997 "Cross correlations and cross spectra for spaced antenna wind profilers", *Radio Science* **32** 967-982
[8] Fedorczak N, Manz P, Thakur S C, Xu M, Tynan G R, Xu G S, and Liu S C 2012 "On physical interpretation of two dimensional time-correlations regarding time delay velocities and eddy shaping", *Phys. Plasmas* **19** 122302
[9] Bendat J S and Piersol A G 2010, "Random Data: Analysis and Measurement Procedures, 4th Edition", (*New York: Wiley Interscience*)
[10] Briggs B H, Phillips G J and Shinn D H 1950, "The Analysis of Observations on Spaced Receivers of the Fading of Radio Signals", *Proc. Phys. Soc. Instrum.*, **63** 106
[11] Conway G D and Elliott J A 1987, "Digital signal processing techniques for plasma dispersion curve measurements", *J. Phys. E: Sci. Instrum.*, **20** 1341
[12] Guo-Wei He and Jin-Bai Zhang 2006, "Elliptic model for space-time correlations in turbulent shear flows", *Physical Review*, **73** 055303
[13] Xin Zhao and Guo-Wei He 2009, "Space-time correlations of fluctuating velocities in turbulent shear flows", *Physical Review*, **79** 046316
[14] Ritz C P, Powers E J, Rhodes T L, Bengtson R D, Gentle K W, Lin H, Phillips P E, Wootton A J, Brower D L, Luhmann N C, Peebles W A, Schoch P M, and Hickok R L 1988, "Advanced plasma fluctuation analysis techniques and their impact on fusion research", *Rev. Sci. Instrum.* **59** 1739
[15] Birkenmeier G, Ramisch M, Fuchert G, Kohn A, Nold B, and Stroth U 2013, "Spatial structure of drift-wave turbulence and transport in a stellarator", *Plasma Phys. Control. Fusion*, **55** 015003
[16] Mahdizadeh N, Greiner F, Happel T, Kendl A, Ramisch M, Scott B D, and Stroth U 2007,

"Investigation of the parallel dynamics of drift-wave turbulence in toroidal plasmas", *Plasma Phys. Control. Fusion* **49** 1005

[17] Vershkov V, Soldatov S, Shelukhin D, and Chistiakov V 1999, "Experimental investigation of ion-temperature-gradient-like turbulence characteristics in t-10 core plasmas with toroidal and poloidal correlation reflectometry", *Nuclear Fusion* **39** 1775

[18] Ribeiro T T and Scott B 2015, "Tokamak turbulence computations on closed and open magnetic flux surfaces", *Plasma Phys. Control. Fusion* **47** 1657

[19] Banon Navarro A, Teaca B, Jenko F, Hammett G W, Happel T, and the ASDEX Upgrade Team 2014, "Applications of large eddy simulation methods to gyrokinetic turbulence", *Phys. Plasmas* **21** 032304

[20] Krämer-Flecken A, Soldatov S, Xu Y, Arnichand H, Hacquin S, Sabot R, and the TEXTOR team 2015, "Long-range correlation properties of quasi-coherent modes at TEXTOR", *New J. Phys.* **17** 073007

[21] Nazikian R, Kramer G J, and Valeo E 2001, "A tutorial on the basic principles of microwave reflectometry applied to fluctuation measurements in fusion plasmas", *Phys. Plasmas* **8** 1840

[22] Vershkov V A, Dreval V V, and Soldatov S V 1999, "A three-wave heterodyne correlation reflectometer developed in the T-10 tokamak", *Rev. Sci. Instrum.* **70** 1700

[23] Krämer-Flecken A, Soldatov S, Vowinkel B, and Muller P 2010, "Correlation reflectometry at TEXTOR", *Rev. Sci. Instrum.* **81** 113502

[24] Soldatov S, Krämer-Flecken A, and Zorenko O 2011, "Low noise Ka-band hopping reflectometer based on Yttrium iron garnet sources at TEXTOR", *Rev. Sci. Instrum.* **82** 033513

[25] Prisiazhniuk D, Krämer-Flecken A, Conway G D, Happel T, Manz P, Simon P, Stroth U, and the ASDEX Upgrade Team 2015, "Application of poloidal correlation reflectometry to study turbulence at ASDEX Upgrade", *Proc. 12th Intnl. Reflectometry Workshop -IRW12 (Jülich)*

[26] Prisiazhniuk D, Krämer-Flecken A, Conway G D, Happel T, Manz P, Angioni C, Stroth U, and the ASDEX Upgrade Team 2016, "Characterization of the turbulence during LOC-SOC transition using Poloidal Correlation Reflectometry at ASDEX Upgrade", *43th EPS Conference on Plasma Physics (Leuven)*

[27] Krämer-Flecken A and Soldatov S 2011, "On the possibility to use Correlation Reflectometry for determination of safety factor at TEXTOR", *10 Internation reflectometry workshop (Padova)*

[28] Poli E, Peeters A G and Pereverzev G V 2001 "TORBEAM, a beam tracing code for electron-cyclotron waves in tokamak plasmas" *Comput. Phys. Commun.*, **136** 90

[29] Hutchinson I H 1992, "One-dimensional full-wave analysis of reflectometry sensitivity and correlations" *Plasma Phys. Control. Fusion*, **34** 1225

[30] Gusakov E Z, G Leclert, I Boucher, S Heuraux, S Hacquin, M Colin, V V Bulanin, A V Petrov, B O Yakovlev, F Clairet and X L Zou 2002 "Small-angle scattering and spatial resolution of fluctuation reflectometry: comparison of 2D analytical theory with numerical calculations", *Plasma Phys. Control. Fusion* **44** 1565

[31] Leclert G, Heuraux S, Gusakov E Z, Popov A Yu, Boucher I and Vermare L 2006 "Full-wave test of the radial correlation reflectometry analytical theory in linear and nonlinear regimes", *Plasma Phys. Control. Fusion* **48** 1389

[32] Conway G D, Schirmer J, Klenge S, Suttrop W, Holzhauer E, and the ASDEX Upgrade Team 2004, "Plasma rotation profile measurements using Doppler reflectometry", *Plasma Phys. Control. Fusion*, **46** 951

[33] Happel T, Conway G D, Hennequin P, Honore C, Giacalone J C, Simon P, Stroth U, Vermare L and the ASDEX Upgrade Team 2013 "The optimized steerable W-band Doppler reflectometer on ASDEX Upgrade: possibilities and issues", *Proc. 11th Intnl. Reflectometry Workshop -IRW11 (Palaiseau)*

[34] Scott B 2001, "Low frequency fluid drift turbulence in magnetised plasmas", *Habilitation thesis*, Duesseldorf Univ. (Germany).

[35] Peeters A G 2000, "Reduced charge state equations that describe pfirsch schlter impurity transport

in tokamak plasma", *Phys. Plasmas* **7** 268

[36] Bortolon A, Camenen Y, Karpushov A N, Duval B P, Andrebe Y, Federspiel L and Sauter O 2012, "Indirect measurement of poloidal rotation using inboard–outboard asymmetry of toroidal rotation and comparison with neoclassical predictions", *Nuclear Fusion* **53** 023002

[37] Viezzer E, Pütterich T, Angioni C, Bermann A, Dux R, Fable E, McDermott R. M. Stroth U and Wolfrum E 2014, "Evidence for the neoclassical nature of the radial electric field in the edge transport barrier of ASDEX Upgrade", *Nuclear Fusion* **54** 012003

[38] Mc Carthy P.J. and the ASDEX Upgrade Team 2012, "Identification of edge-localized moments of the current density profile in a tokamak equilibrium from external magnetic measurements", *Plasma Phys. Control. Fusion* **54** 015010

[39] Silva A, Cupido L, Manso M, Serra F, Nunes I, Santos J, Varela P, Vergamotta S, Meneses L, Grossman V, Silva F, Loureiro C, Nunes F, Kurzan B, Suttrop W 1999, "Microwave reflectometry diagnostic for density profile and fluctuation measurements on ASDEX Upgrade", *Rev. Sci. Instrum.* **70** 1072

[40] Graça S 2009, "MHD and fast particle mode studies using fast frequency hopping reflectometers on the ASDEX Upgrade tokamak", *PhD thesis*, Universidade Técnica de Lisboa

[41] Strumberger E, Gunter S, Schwarz E, Tichmann C and the ASDEX Upgrade Team 2008 "Fast particle losses due to NTMs and magnetic field ripple", *New Journ. of phys.*, **10** 023017